Essential Readings in Light Metals: Aluminum Reduction Technology.
Edited by Geoff Bearne, Marc Dupuis and Gary Tarcy.

From 110 to 175 kA: Retrofit of VAW Rheinwerk
Part I: Modernization Concept

D. Vogelsang, I. Eick, M. Segatz, Ch. Droste
VAW Aluminium-Technologie
53117 Bonn, Germany

Abstract

Modernization of the 210,000 tpy VAW Rheinwerk smelter includes installation of point feeder, alumina conveying system, state-of-the-art pot control system and foresees an increase in amperage of up to 175 kA. For the modernized pots concepts for the potlining as well as for improvements of the busbar system were developed based solely on computer simulations.
For the layout of the potlining a new three-dimensional thermo-electric cell model was applied that allows prediction of side ledge contours as well as heat and voltage balances. Based on this model the choice of semi-graphitic vs. fully graphitized cathode blocks was evaluated with respect of the anticipated increase in system amperage. Temperature fields and side ledge contours predicted are in good agreement with measurements. The busbar system, designed originally for a current load of 110 kA, was improved in a very efficient manner to cope with the higher amperage. Magneto-hydrodynamic simulations predicted and plant measurements demonstrated significant improvements in cell stability and performance.

Introduction

The Rheinwerk Smelter located near Dusseldorf is one of the major primary aluminium sources for VAW Aluminium AG. The smelter was founded in 1960 with end-to-end pots and a prebaked continuous anode technology operating at an amperage of 110 *kA*. In 1981-1984 the potrooms were modernized by introducing prebaked discontinuous anodes. At present the nameplate capacity of the 474 cells operating in three systems at 163 *kA* is 210,000 tpy. In an attempt to increase productivity and to improve operational results of the smelter a modernization concept was developed in 1994 and ten pilot pots were taken into operation in 1995 to demonstrate the potential of the existing pots. The retrofit project includes the following measures:

- Improved busbar system
- Point feeder and alumina conveying system
- Newest generation of the *ELAS* pot control system of VAW.
- New pot shell and potlining in the course of maintenance repair

After one year of successful operation the complete modernization of the Rheinwerk smelter according to this concept was decided in 1996. The total investment costs for this retrofit will be 40 Mio DEM and will be amortized within a period of four years. This paper describes the development of the conceptual design for the new pot shell and potlining based on a newly developed tool for the prediction of heat and voltage balance. The impact of fully graphitized cathodes and the anticipated increase in current load to 175 *kA* as well as measures for the magneto-hydrodynamic improvement of the cell will be elucidated.

Basics of the Thermo-Electric Model

For the calculation of heat and voltage balances, a three-dimensional thermo-electric model is applied that replaces the former two-dimensional tool [1]. It is based on the Finite Element code *ANSYS* (SAS IP, Inc.) and follows a similar approach published by Dupuis and Tabsh [2] for the thermo-electric model of the cathodic region of reduction cells. The equations for heat and electric current flow are solved simultaneously. *Figure 2* demonstrates the topology of the solution domain. Typical simulations were done for a slice of the cell containing half an anode and for the cathodic part half a cathode block. These two components of the model have a common interface denoted as **(A)** in *Figure 1*. The nodes within this interface are coupled by the corresponding temperatures. The location of this interface is chosen to be practically adiabatic, hence, the heat flow between both sub-models can be nearly neglected as will be shown by the heat balances of both sub-models given in *Table 2*. The model contains all relevant structural parts like anode stem, yoke, the cast between studs and anode carbon block, side lining as well as insulating materials, cathode block, collector bar and the cast connecting the collector bar with the cathode block. The anode carbon block is rounded to reflect the burn-off. The steel shell with realistic dimensions for the cradle builds up the periphery at the side and bottom.

The interior of the cell with the liquid metal and electrolyte is not within the solution domain of the thermal problem. It is

modeled via special thermal boundary conditions in the regions **(B-E)**, c.f. *Figure 1.* For the determination of the anodic voltage drop including fanning effect the liquid electrolyte layer is incorporated as a pure electric component into the model.

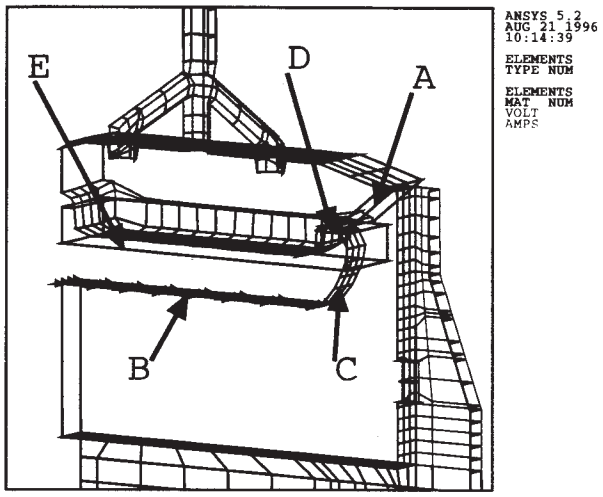

Figure 1: Boundary conditions of the thermo-electric model.

The solution domain is discretized by a FORTRAN coded preprocessor into typical 2,500 thermo-electric elements from a parametric description of the dimensions of all relevant key components. Surface and shell elements build up the periphery of the domain. They are used for the definition of the boundary conditions as well as for the determination of heat fluxes.

The temperature-dependent thermal and electrical conductivities used for the structural parts of the model are taken from the VAW data base. They usually reflect medium aged materials and correspond to typical pot characteristics. For the electrical potential the following two boundary conditions are applied: at the upper surface of the anode stem current with the nominal current density is entering the model and at the interface between electrolyte and metal an equipotential surface with the arbitrary potential zero is defined. The cathodic boundary condition consists of an equipotential surface on top of the cathode block and a specified current density at the outer end of the collector bar. A set of thermal boundary conditions is applied to the outer surface of the solution domain that was determined by numerous plant measurements. These heat transfer coefficients combine convective and radiative mechanism. Typical ambient temperatures are assumed: 100°-190°C for the yoke and alumina covering, +30°C for the pot shell.
For the interior of the cell a defined superheat for the electrolyte and liquid metal is applied. A special set of heat transfer coefficients from bath to side ledge, bath to anode, metal to side ledge and metal to cathode carbon block is used. For the gas filled gap **(D)** in *Figure 1* beneath the top crust a constant radiating temperature of bath temperature is assumed.

The model is controlled by three essential values, namely total cell voltage, superheat and side ledge offset. By defining one of them the others can be calculated by an iterative procedure.

a) Prediction of total cell voltage and superheat for a predefined intersection of the side ledge and cathode carbon block. The results given in the next sections are obtained applying this computational variant.

b) Prediction of total cell voltage and side ledge for a given superheat.

c) Prediction of superheat and side ledge for a given cell voltage.

In the first case the simulation starts with a fixed intersection of the side ledge on the cathode carbon block and a reasonable contour for the side ledge. The liquidus temperature of the side ledge is determined according to the bath composition. During the iteration the shape of the side ledge is deformed in such a way that the temperatures equalize the liquidus temperature. The superheat is modified from one iteration step to the next until the desired side ledge offset is obtained. As the superheat is modified during the solution procedure, the thermal energy demand of the cell with a stable side ledge is determined.

After each iteration the heat losses and the voltage balance of the complete cell are calculated from the heat losses of the slice model by weighting the anodic and cathodic heat losses with the number of anodes and cathodes in the real cell. Heat losses of the side walls of the steel shell are weighted with the quotient of slice thickness and circumference of the cell and corrected with a factor to account for the temperature drop at the cell edges. The justness of this computational method was validated by simulations of other cells based on an analogous slice model and a three-dimensional corner model comprising each two anode and cathode blocks. The heat loss of the complete cell determined in this way is the sum of the JOULE heat generated in anodes and cathodes and the heating power of the bath transported through the boundaries **(B-E)** in *Figure 1.* The JOULE heat generated in the structural parts of anodes and cathodes is directly calculated by the FEM code *ANSYS* from the solution of the electric potential problem. By dividing through the actual current the voltage drops in these structural parts are obtained. In the same way the bath voltage is obtained from the heating power. Hence, together with the external voltage drop of the busbar system a complete voltage balance of the pot under stable thermal conditions is obtained.

Heat and Voltage Balance Calculations

The three systems of Rheinwerk Works comprise three major basic types of reduction cells that reflect successive generation of pots. They differ in dimensions of the cathode shell, number of cathodes as well as potlining design. Heat and voltage balance calculations were performed for all the different cell types, although results are presented here for the newest generation of cells, only. Some basic data for this 3rd cell generation are given in *Table 1.* The cells are equipped with SiC side slabs and a strong insulating cathodic potlining. In the course of

Table 1: Basic Data of Anodes and Cathodes

Pot shell $(L \times W \times H)$	mm	$9,000 \times 4,100 \times 1460$
Anodes	-	20
$(L \times W \times H)$	mm	$1,480 \times 745 \times 600$
Yoke ϕ	mm	150
Studs	-	3
Cathodes	-	21
$(L \times W \times H)$	mm	$3,355 \times 350 \times 450$
Collector bars $(W \times H)$	mm	90×220

the Conceptual Design study the impact of different cathode qualities on heat and voltage balance was analyzed: an amorphous cathode with 30 % graphite, e.g. KA23 (VAW Carbon) referred in the following as semi-graphitic and a fully graphitized cathode, e.g. KA4 quality. Calculations were performed for current loads up to the scheduled amperage of 175 kA.

Results for Amorphous Cathodes

For the steel shell of the new pots a stiff cradle-type construction was developed, similar to the one published before for another 165 kA pot [3]. The steel construction is fully welded with cradles located beneath each adjacent collector bar. The dimensions of the construction were optimized with respect of weight and stiffness applying a statical Finite Element analysis.

The calculated temperature field for semi-graphitic KA23 cathodes and an amperage of 163 kA is given grey-coded in *Fig. 2.* For the anodic part the cooling effect of studs and yoke is obvious. The temperature field of the cradle demonstrates the cooling effect on the steel shell. Due to the strong bottom insulation the cradle parts beneath the pot appear cooler. Minimum temperature for the cathode block was calculated to be $739°C$, although the typical temperature range is between $850°C$ and $950°C$. Maximum temperatures for the shell sides are calculated to be 305 $°C$, much higher than for the bottom plate ($94°C$). Shell temperatures from two different measurement campaigns are plotted together with the calculated temperature profile at the midst of the slice model as well as for the symmetry plane in *Fig. 3.* Calculated and measured shell temperatures are in good agreement.

The predicted side ledge protects the ramming paste sufficiently. The calculated contour of the ledge agrees with plant measurements of the demonstration pots as can be seen from *Fig. 4.*

There is a certain difference in the mean contour for the aisle and window side that might be caused by the fluid field of bath and metal and/or different heat transfer conditions for both sides.

A detailed heat balance for the demonstration pots with semi-graphitic KA23 cathodes as well as the calculated heat balance for fully graphitized cathodes (KA4) is given in *Table 2.*

The JOULE heat generated in the electric conducting parts as well as the heat transferred from bath and metal to the anodic and cathodic sub-model is denoted in the table as *"Input"*. Convective and radiative heat losses over the boundary of the slice model are summarized as *"Output"*. It might be interesting to look at the grey-coded distribution of anodic and cathodic JOULE heat generated, c.f. *Fig. 5.*

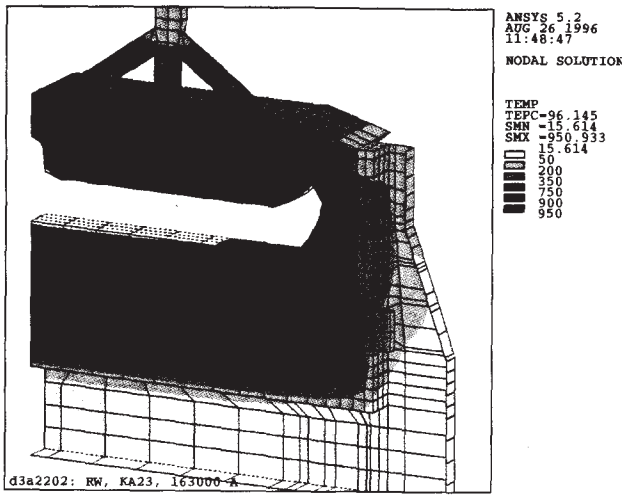

Figure 2: Temperature field, KA23 cathodes @ 163 kA

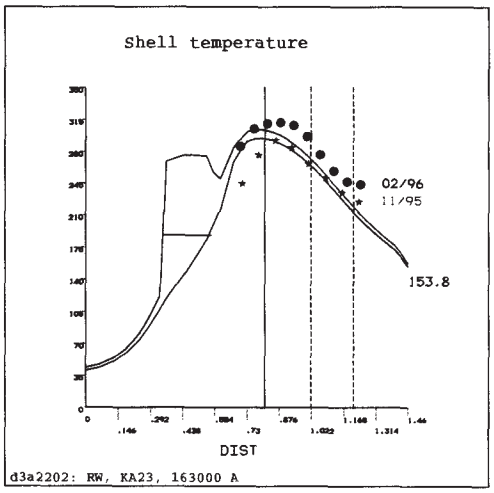

Figure 3: Shell temperatures, KA23 cathodes @ 163 kA

In the anodic part due to the high current density large values are calculated for the upper part of the yoke right beneath the anode rod. Values > 200 kW/m^3 are calculated for the bath beneath the anode. In the cathodic part due to horizontal current density components relatively large values are found in the upper part of the cathode block in front of the side ledge. For the collector bar maximum values are calculated right behind the end of the cathode blocks. This maximum is caused by the gradual increase in current density and the steady decrease of electrical resistivity corresponding to the decreasing

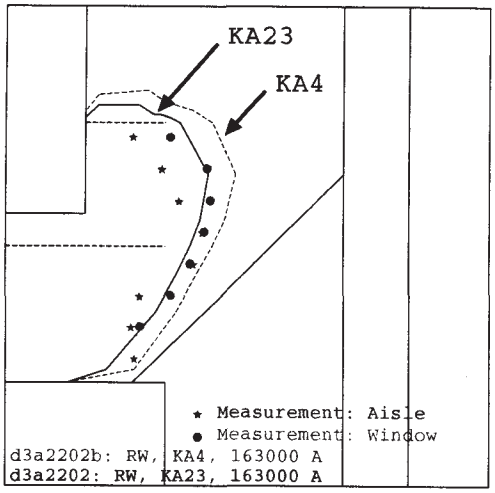

Figure 4: Calculated and measured side ledge, KA23 cathodes @ 163 kA

Table 2: Heat Balance KA23, KA4 Cathodes in $[kW]$ @ 163 kA

item	KA23, 163 kA Input	KA23, 163 kA Output	KA4, 163 kA Input	KA4, 163 kA Output
Anode rod	2.1		2.1	
Yoke, studs & casting	25.9		25.9	
Anode block	36.4		36.4	
Bath → Anode	89.1		90.6	
Anode rod		16.1		16.1
Yoke		60.0		60.2
Covering		79.1		81.2
Σ anodic part	153.2	155.2	155.0	157.5
Bath/metal → Cathode	160.5		195.6	
Cathode carbon	13.0		5.6	
Collector bar & casting	25.5		24.5	
Deckplate		5.5		6.2
Shell, side		118.7		136.8
Shell, bottom		31.3		33.6
Collector bar		41.7		46.5
ΣCathodic part	198.9	197.2	225.7	223.1
ΣΣHeating power	**352.4 kW**		**380.7 kW**	

temperatures of the steel bar.

The total anodic JOULE heat sums up to 64 kW corresponding to an anodic voltage drop of 395 mV, a value typically found in plant measurements for the demonstration pots. The anodic JOULE heat contributes only 42 % to the total anodic heat input of 153 kW. The other 58 % are transferred from the bath to the anode carbon block. This discrepancy between JOULE heat production and heat transferred from the interior of the cell is even larger for the cathodic sub-model. Only 38 kW are produced due to current flow in the cathode carbon block, collector bar and casting between collector bar and cathode block. Some other 161 kW or 80 % of the total heat input of 199 kW is transferred from bath and metal to the cathode. The voltage drop of the cathodic sub-model calculated from the JOULE heat

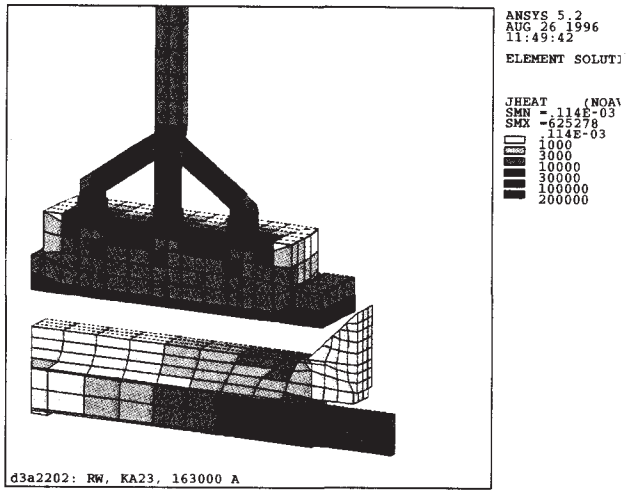

Figure 5: JOULE heat $[W/m^3]$, KA23 cathodes @ 163 kA

is 236 mV. Plant measurements indicate that typical cathode voltage drops for younger pots are about 300 mV. The difference can be explained by the fact that the measuring points include parts of the external busbar system. This difference is in the order of 70 mV, hence cathodic voltage drops agree with plant measurements.

The total cell voltage was calculated to be 4.43 V for the actual amperage of 163 kA including a voltage drop of 280 mV for the busbar system and 50 mV as contribution of anode effects. The anode-cathode-distance (a.c.d.) was estimated to be 62 mm. The specific energy demand of the demonstration pots was calculated to be 14.1 $kWh/kg\ Al$ for a current efficiency of 93.5 %.

The scheduled increase in amperage up to 175 kA will have only a minor influence on the temperature field. Minimum cathode temperatures increase from 739°C to 745°C while shell and cradle temperatures are not significantly modified. The total heat losses of the cell are nearly identical for both amperages. The increase in JOULE heat produced in anodes and cathodes is compensated by a decrease in the heat transferred from the interior of the cell to both sub-models. The total anodic JOULE heat increases by about 10 kW while the heat transferred from the bath is reduced by 6 kW. Cathodic JOULE heat increases by 6 kW and the heat transferred from bath and metal is reduced by the same amount. The anodic and cathodic voltage drops increase by 30 and 17 mV, respectively. On the other hand the bath voltage is reduced by 170 mV. The total cell voltage for the scheduled amperage of 175 kA will be 4.33 V corresponding to a specific energy demand of 13.8 $kWh/kg\ Al$.

Fully graphitized Cathodes

The evaluation of the heat and voltage balance with fully graphitized cathode blocks was performed with the same slice

model as used as for the semi-graphitic case.
For the cathode carbon block the thermal conductivity was increased by a factor of 2.8, the electrical resistivity was reduced by a factor of 5.

The calculated temperature field for the actual amperage of 163 kA is given in *Fig. 6* and should be compared with the semi-graphitic case in *Fig. 2*.
The anodic temperature field is nearly identical for both cases. A slight increase in the anode temperatures can be seen at the short sides of the anode carbon blocks. The heat balance for the anodic part is not modified significantly compared with the semi-graphitic case, c.f. *Table 2*. This can be explained by the fact that the quasi-adiabatic interface (**A**) in *Fig. 1* decouples the anodic sub-model from changes in the cathodic region.
Much more uniform temperatures are predicted for the cathode carbon block due to the better heat conductivity. The minimum cathode temperature increases from 739$°C$ for the semi-graphitic case to 840$°C$. The larger cathode temperatures result in higher shell temperatures at the long side of the cell. Maximum temperatures increase from 305$°C$ to 352$°C$ while bottom temperatures compare with the semi-graphitic case. The increase in shell temperatures give rise to larger heat losses at the shell sideplates and the cradles at the long side. The total cathodic heat losses increase from 197 kW to 223 kW. Due to the better electrical conductivity the JOULE heat produced in the cathode blocks reduces from 13 kW to 5.6 kW. The reduced resistivity favours the take up of the current at the cooler parts of the collector bars. Hence, the JOULE heat produced in the collector bars and casting is reduced from 25.5 kW to 24.5 kW, too. The total voltage drop in the cathodic submodel is lessened from 236 mV to 186 mV, corresponding to cathodic voltage drops of about 255 mV for the real pots. The reduced cathodic JOULE heat production and the increase in heat losses must be compensated by an increased bath voltage, hence a larger a.c.d. to ensure a side ledge contour comparable with the semi-graphitic case. Bath voltage rises from 3.47 V to 3.69 V and accordingly the total pot voltage increases from 4.43 to 4.61 V for the actual current load of 163 kA. Due to the fact that the amplified heat losses of the cathode are compensated by additional heating power in the bath region, the side ledge is weakened compared to the semi-graphitic case, c.f. *Fig. 4*.

For the scheduled amperage of 175 kA heat and voltage balances are modified in a similar way as explained for the semi-graphitic case. The temperature field as well as anodic and cathodic heat losses remain nearly unchanged. The increase in JOULE heat produced allows for a decrease in the a.c.d. and bath voltage. The total pot voltage predicted for 175 kA is 4.49 V and as for the actual amperage the specific energy demand is about 0.5 $kWh/kg\ Al$ higher than for the semi-graphitic case.

Measures to reduce the excess of heat losses of the fully graphitized cathode could be either a reduction in length of the cathode carbon blocks or a further increase in the current load. Shortening of the cathodes is unfavourable because the cathode geometry is more or less dictated by the dimensions of the anode table. A further increase of current load would result in stronger magneto-hydrodynamic instability and metal velocity. Therefore the modernized Rheinwerk pots will be equipped

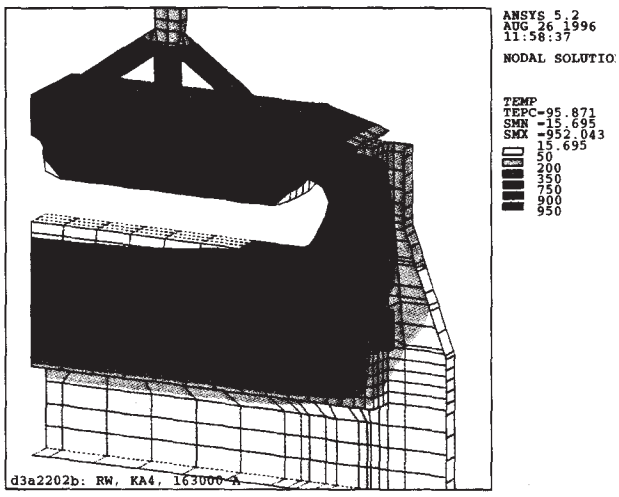

Figure 6: Temperature field, KA4 cathodes @ 163 kA

with semi-graphitic cathodes.

Improved Busbar System

The original busbar system of the Rheinwerk pot is symmetric in design. No measures to compensate the magnetic influence of the adjacent potline are taken. Two cathodic busbars pick up each 14 and 7 collector bars, resulting in the following current distribution of the four risers

Plant measurements [4] indicated for this configuration a distinct tendency to build up MHD instabilities with typical periods of 40 s. The MHD stability model developed by VAW was verified using these plant measurements [5]. Some characteristic MHD parameter of this pot as predicted by the published MHD tools [6, 7, 8] are given in *Table 3*.

Table 3: MHD Values: Original and Improved Busbar System

		163 kA original	163 kA improved	175 kA improved
B_z offset	G	24	12	13
v_{mean} metal	cm/s	8	9	10.0
v_{max} metal	cm/s	17	25	26
Δh	cm	3.7	4.3	4.9
Growth factor	$1/s$	0.042	0.015	0.018
Period	s	40	33	32

The offset of the vertical magnetic B_z component due to the adjacent line is calculated to be 24 G. This offset gives rise

to MHD instabilities. The worst eigen-mode with a period of 40 s was predicted to have a growth factor of 0.042 [1]. Mean and maximum metal velocities of the original cell are moderate. The metal pad heaving has a maximum in the cell center. Maximum height is calculated to be $+1.2$ cm, minimum values are calculated for the downstream side as -2.5 cm.

This busbar system was improved by simply cutting off the downstream riser opposite to the adjacent potline and connecting the two cathodic busbars on this side. The resulting current distribution of the remaining three risers is as follows:

Due to this modification the offset of the vertical magnetic field component is reduced by a factor of two. The predicted growth factor of the most prominent eigen-mode is reduced to a feasible value of 0.015 s^{-1}. Indeed, for the demonstration pots with this modified busbar system MHD stability was strongly improved and metal pad rolling has not been detected anymore.

The time-averaged mean metal velocity is slightly increased. Maximum velocities of the fluid field limit a further increase in amperage beyond 175 kA. The metal pad heaving increases as measured *peak-to-peak*, however beneath the anode table moderate values of $+0.9$ cm are predicted. Minimum values are calculated for the upstream side outside the anode table with values of -3.4 cm.

Conclusions

A fully three-dimensional Finite Element model to predict heat and voltage balances for reduction cells was developed. Plant measurements agree with the predicted temperature field and side ledge contour. This tool was applied for the development of a new pot generation for the Rheinwerk Smelter. These pots will be equipped with point feeder, an alumina conveying system as well as the new *ELAS* pot control system. The amperage will be increased from 163 kA to 175 kA in the course of the modernization.

During the Conceptual Design study the impact of fully graphitized cathode carbon blocks compared with semi-graphitic blocks was evaluated. The results can be summarized as follows:

- The anodic heat losses of the cells are not significantly influenced by the introduction of fully graphitized blocks.
- Much more uniform temperatures are predicted for the fully graphitized blocks with minimum temperatures up to $840°C$ compared with $739°C$ for the semi-graphitic blocks.
- Cathodic voltage drops are improved by 50 mV, however this reduced voltage drop is jeopardized by the tremendous increase in bath voltage needed to compensate the increased cathodic heat losses at the long side of the cell. For the actual current load of 163 kA the total cell voltage was predicted to be 4.61 V compared with 4.43 V for the semi-graphitic case.
- For the anticipated increase of amperage up to 175 kA the modernized cells will be equipped with semi-graphitic cathodes. The predicted total cell voltage will be 4.33 V and the specific energy demand was calculated to be 13.8 kWh/kg Al.

The original symmetric busbar system was improved by converting to a three-riser configuration and connecting two cathodic busbars. This results in a reduction of the vertical component of the magnetic field by a factor of two and reduces the level of MHD instabilities. For demonstration pots equipped with this improved busbar system metal pad rolling has not been observed until now.

[1] **The growth factor is the reciprocal time needed to double the amplitude of the corresponding eigen-mode. Hence, large values indicate a marked tendency to build up instabilities, c.f.** SEGATZ, DROSTE **[5].**

References

[1] H. Pfundt, D. Vogelsang and U. Gerling, *Calculation of the Crust Profile in Aluminium Reduction Cells by Thermal Computer Modelling*, Light Metals 1989, pp. 371-377.

[2] M. Dupuis and I. Tabsh, *Thermo-electric Analysis of Aluminium Reduction Cells*, Proc. 31st. Annual Conference of CIM, Light Metals Section (1992), 55-62.

[3] D. Vogelsang, Ch. Droste, M. Segatz and I. Eick *Retrofit of Søderberg Smelter at Alusaf Bayside Plant - Part 1: Conceptual Design and Engineering*, Light Metals 1996, pp. 327-333.

[4] G. Loßmann, *"Utilization of various combined measurements in reduction cells for operational improvement"*. Light Metals 1992, pp. 441-447.

[5] M. Segatz and C. Droste, *Analysis of Magneto-hydrodynamic Instabilities in Aluminium Reduction Cells*, Light Metals 1994, pp. 313-322.

[6] M. Segatz and D. Vogelsang, *Effect of Steel Parts on Magnetic Fields in Aluminum Reduction Cells*. Light Metals 1991, pp. 393-398.

[7] D. Vogelsang and M. Segatz, *Simulation Tools for the Development of High-Amperage Reduction Cells* Light Metals 1991, pp. 375-379.

[8] D. Vogelsang, *Application of Integrated Simulation Tools for Retrofitting Aluminium Smelters*, 4th. Australasian Aluminium Smelter Techn. Workshop, 25-30 October 1992, pp. 641-643.